Pergamon

Phys. Chem. Earth (A), Vol. 24, No. 7, pp. 639–644, 1999

1464-1895/99/$ - see front matter

PII: S1464-1895(99)00093-9

New Algorithms in 3D Image Analysis and their Application to the Measurement of a Spatialized Pore Size Distribution in Soils

J. F. Delerue[1, 2], **E. Perrier**[2], **Z. Y. Yu**[1] **and B. Velde**[3]

[1]LIAMA, Sino-French Laboratory of Research in Computer Science, Control and Applied Mathematics, Institute of Automation, Chinese Academy of Sciences, P.O. Box 2728, Beijing 100080, People's Republic of China
[2]LIA, ORSTOM, 32 avenue Henri Varagnat, 93143 Bondy Cedex, France
[3]Laboratoire de Géologie, ENS, URA 1316 CNRS, 24 rue Lhomond, 75231 Paris, France

Received 24 April 1998; revised 1 December 1998; accepted 4 December 1998

Abstract. We introduce a skeletization method based on the Voronoi diagram to determine local pore sizes in any porous medium. Using the skeleton of the pore space in a 3D image of the porous medium, a pore size value is assigned to each voxel and a reconstructed image of a spatialized local pore size distribution is created. The reconstructed image provides a means for calculating the global volume versus size pore distribution. It is also used to carry out fluid invasion simulation which take into account the connectivity of and constrictions in the pore network. As an example we simulate mercury intrusion in a 3D soil image.

1 Introduction

The concept of pore size distribution is widely used in soil science to characterize different types of soils or to characterize dynamic evolution within a given soil (e.g. Velde et al., 1996). It is also widely used in theoretical modeling or specific applications to infer soil hydraulic and other properties of soil behavior (e.g. Dullien, 1992; Perrier et al., 1996, 1998). Specific devices (mercury porosimeters) have been developed to provide indirect measurements of the pore size distributions in small soil cores and numerous specific experiments are carried out to estimate pore size distributions either in the field or in the laboratory (e.g. Fies, 1992; Zida et al., 1996). Image analysis has also been used to measure pore size distributions directly on soil images, extensively in 2D (Hallaire and Curmi, 1994), using available computer softwares, and more recently from 3D soil images using specific algorithms based on morphological analysis (Moreau et al., 1999).

3D soil images alone can give us an insight about the connectivity of the pore space, which have proved to be the key factor as regards soil hydraulic properties. Theoretical studies of pore networks modeling soils (Perrier et al., 1995) (or any kind of porous media (Lenormand et al., 1988)) show that a pore size distribution cannot completely explain fluid flow if we neglect the spatial distribution of the different pore sizes: given the same distribution of pore sizes (% of the total pore volume in different classes of sizes) and local flow properties, the macroscopic behavior may vary strongly according to connectivity, i.e., the way these sizes are distributed in space and how they are related to each neighbor, which determine fluid paths.

Our goal in this paper is to go beyond the mere measurement of pore size distributions and to obtain a reconstructed image of the spatialized pore size distribution, i.e. a map of pore sizes, that may be useful to carry on numerical experiments of fluid flow on improved pore network models.

Section 2 presents our theoretical approach and the algorithms that have been developed in this framework. Section 3 exhibits an example of application on real data where a virtual experiment of mercury invasion is performed. Section 4 summarizes our preliminary conclusions about this on-going research.

2 Theory and methods

2.1 Local pore size and spatialized pore size distribution definitions.

The pore concept refers generally to models representing the voids in a porous medium as a set of elementary units with simple geometrical shapes, e.g. a bundle of cylindrical tubes of various apertures. Here the pore size is simply the radius of the cylinder. This size r is then linked to the capillary pressure h necessary to displace a fluid through this tube, according to the Young–Laplace Law (e.g. de Marsily, 1986; Washburn, 1921):

$$h \sim \frac{k}{r} \qquad (1)$$

where k is a numerical constant depending on the fluids, the medium, the experimental conditions etc., with details going beyond the scope of the present paper.

In a real pore space, the complex continuous geometry does not allow a precise definition of a pore except as a local

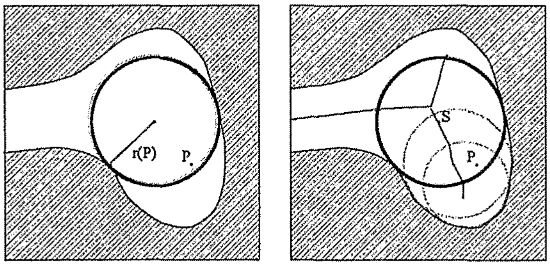

a b

Fig. 1. a) The local pore size $r(P)$ for any point P in the pore space $\mathcal{P}$ is defined as the radius of the largest ball (circle on the picture) including P and included in $\mathcal{P}$. b) $r(P)$ is calculated as the radius of the maximal ball (black circle) centered on a point S of the skeleton $\mathcal{S}$.

region of the pore space: there are few well specified objects with specific sizes. We will define locally a pore size as the local distance between the solid parts surrounding a point located in the pore space. From considerations related to our vision of the link between this local size and the local properties of fluid flow, we will use here the following definition: for any point P located in the pore space $\mathcal{P}$, let us define the local pore size $r(P)$ as the radius of the greatest ball (circle in 2D, sphere in 3D) included in the pore space and including P.

$$r(P) = \max\{r \mid \mathcal{B}(C,r) \subset \mathcal{P}, P \in \mathcal{B}(C,r)\} \tag{2}$$

The spatialized pore size distribution $\mathcal{M}$ is then defined as the following set of geometrical information (points+associated local sizes):

$$\mathcal{M} = \{P, r(P) \mid P \in \mathcal{P}\} \tag{3}$$

i.e. a set of (x,y,z,r(x,y,z)).

First $\mathcal{M}$ includes all the necessary information to calculate the global pore size distribution that may be defined as a continuous density function of the pore volume with respect to the size r.

Second $\mathcal{M}$ includes a map of local pore sizes that will be useful to characterize the connectivity of the pore space.

2.2 From a real soil image towards a reconstructed image of its spatialized pore size distribution $\mathcal{M}$

In order to determine the local size $r(P)$ in $\mathcal{M}$ defined by Eq. (2), it is necessary to define specific algorithms using explorations around P : Calculations of successive balls centered upon any point in the pore space could be used but the tests are long and complicated. Our method uses a skeletization of the pore space. This reduces the number of points investigated in the image. One morphological definition of the skeleton $\mathcal{S}$ of the object $\mathcal{P}$ is useful. $\mathcal{S}$ is the set of points made of all the centers S of all the maximal balls $\mathcal{B}(S,r)$ included in $\mathcal{P}$ (Schmitt and Mattioli, 1994; Xia, 1989) (A maximal ball means that we cannot find a bigger sphere including $\mathcal{B}$ and included in $\mathcal{P}$). This means that we can reduce our search of the maximal balls in Eq. (2) by considering only the maximal balls whose centers are defined by the skeleton. Instead of considering each point P in $\mathcal{P}$ and calculating $r(P)$, we will scan all the maximum balls centered upon a point S of the skeleton to assign a value $r(P)$ to the points P covered by this ball. In this iterative process, a point P may be first assigned a $r(P)$ value by a ball covering it, then if a larger ball can occur, still including P, the value $r(P)$ will be increased accordingly (cf. Fig. 1b).

More precisely, the algorithm to determine $r(P)$ proceeds with the following steps:

1 The skeleton $\mathcal{S}$ of $\mathcal{P}$ is extracted and then the maximum balls are calculated.
2 An initialisation of the $r(P)$ values is made: $\forall P \in \mathcal{P}, r(P) = 0$
3 Skeleton points are scanned: for each point S of $\mathcal{S}$, a sub-set of point P_i of the pore space $\mathcal{P}$ is covered by the associated maximal ball $\mathcal{B}(S,r)$: if $r > r(P_i)$, then $r(P_i) = r$. (4)

At the end of the process, each point P of $\mathcal{P}$ is thus assigned a given local pore size $r(P)$, which defines the spatialized pore size distribution $\mathcal{M}$.

2.3 Computation of the skeleton of an heterogeneous 2D or 3D object

The skeleton $\mathcal{S}$ of the pore space $\mathcal{P}$ is rather classically computed from the Voronoi diagram $\mathcal{V}$ for the boundary of the object $\mathcal{P}$. $\mathcal{P}$ is a finite set of points (voxels) in a binary (solids / voids) image of a porous medium. The Voronoi diagram is determined using a new method by taking advantage of this discrete configuration of points. A very fast algorithm has been implemented in 3D by our team (Yu et al., 1998) using an extension of the method proposed in 2D by (Guan and Ma, 1998). The seeds or points investigated are all the voxels located on the boundary of the object $\mathcal{P}$. The Voronoi process partitions the pore space in polyhedric areas of greatest proximity to these seeds (Fig. 2a and b). The Voronoi diagram $\mathcal{V}$ is made of all the edges of these areas. By construction, all the points V in $\mathcal{V}$ are located equidistant from the two nearest seeds A and B (Fig. 2a and b) on the boundary of $\mathcal{P}$. Theoretically, the skeleton $\mathcal{S}$ of $\mathcal{P}$ can be also defined as the median line (e.g. Pieritz and Philippi, 1995) between opposite boundaries of $\mathcal{P}$, thus $\mathcal{S}$ is a sub-set of $\mathcal{V}$.

The next step deals with the calculation of $\mathcal{S}$ (Fig. 2d) by finding the appropriate subset of $\mathcal{V}$. For each point V of $\mathcal{V}$, we have to decide if it belongs to $\mathcal{S}$. Our method consists of calculating the angle $\widehat{AVB}$ between V and the nearest seeds A and B used in defining the Voronoi diagram: if A and B are located on the same side of the boundary of the pore space, this angle will be small (Fig. 2c), if A and B are located on opposite sides of the boundary, the angle $\widehat{AVB}$ will be large (Fig. 2b). A point V belongs to the median line if the angle $\widehat{AVB}$ is large enough (Fig. 2d). We use this empirical method (tuning) to extract the median line by selecting

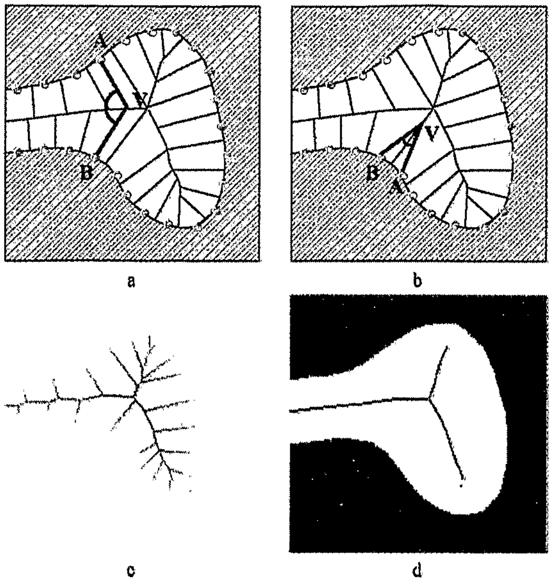

Fig. 2. a, b) Thin lines show Voronoi diagram $\mathcal{V}$, made of points equidistant to 2 seeds (dots) on the pore boundary. a) A point V on $\mathcal{V}$ forms a large angle $\widehat{AVB}$ with its nearest seeds A and B on the pore boundary. b) As in Fig. 2a but where $\widehat{AVB}$ is a small angle. c) A map of the values of the angle $\widehat{AVB}$ for each point of the Voronoi diagram $\mathcal{V}$. Lightest shading shows smallest angles. d) Derived skeleton of pore.

the points V associated to $\widehat{AVB} > K$, where the constant K is chosen to reduce disconnected areas in the median line as well as small appendicies ("*barbules*") or noisy areas around the median line.

$$\mathcal{S} = \{V \mid V \in \mathcal{V}, \widehat{AVB} > K\} \qquad (5)$$

where K is an empirical tuning constant, and A, B are the nearest seeds of V in $\mathcal{V}$.

Moreover, the distance $d = VA (= VB)$ gives the radius of the maximal ball centered upon V needed to complete the algorithm described in Sect. 2.2 Eq. (4). The pore sizes are thus defined as measurable Euclidean distances.

2.4 Examples on synthetic media.

Our method was first tested on simple assemblages of cylinders (Fig. 3a and b) and the radius given by construction were correctly computed in the reconstructed image of $\mathcal{M}$ showing visually the different pore sizes (Fig. 3e and f).

2.5 . First results and sensitivity analysis

If the skeleton was perfect, all the points P of the pore space would be covered by a maximal ball centered on the skeleton and the renconstructed image $\mathcal{M}$ would concern all the points of the pore space $\mathcal{P}$ associated with exact pore sizes. If we

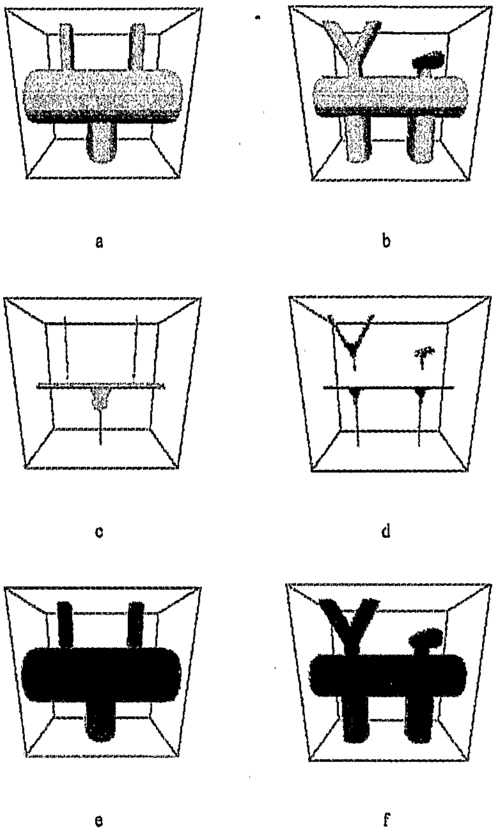

Fig. 3. Examples of the extraction of $\mathcal{M}$ from a simple assemblage of volumes. a, b) Simple volume assemblage $\mathcal{P}$. c, d) Skeleton of pore space $\mathcal{S}$. e, f) Representation of $\mathcal{M}$ with different colors associated to 3 classes of local size: red is the smallest size, green the intermediate size and blue the largest size.

keep too many points in the skeleton (the theoretical skeleton $\mathcal{S}_{th}$ included in our numerical estimation $\mathcal{S}_{est}$, i.e K too low in Eq. (5)) our method is not optimal, but the result is the same. If some points are missing in the skeleton ($\mathcal{S}_{est}$ included in $\mathcal{S}_{th}$, K too high in Eq. (5), two sorts of errors can occur. On the one hand, since a maximal ball may be missing, the local pore size in $\mathcal{M}$ may be somewhat underestimated. On the other hand, some points P of the pore space may be covered by no balls, and these points will not appear in the reconstructed image $\mathcal{M}$. The best results were obtained fixing the K parameter in Eq. (5) at 70°. Our algorithm to extract the skeleton was found to be good enough for our present purpose. The algorithm runs very rapidly and its runtime is simply proportional to the size of the object.

The sensitivity analysis is used to compare the amount of discrepency between $\mathcal{M}$ and $\mathcal{P}$, both on synthetic case studies and on real images.

1. A visual comparison is made with well-known synthetic images (Fig. 3)
2. Computation of the relative error of the total volume (number of voxels) in the original image $\mathcal{P}$ and in the reconstructed image $\mathcal{M}$ (Fig. 4) is made.
3. The process is repeated with different orientations of the image

Our first tests exhibited very encouraging results. Moreover, on all our examples, the connectivity of $\mathcal{M}$ is analogous with the initial connectivity of $\mathcal{P}$, despite a somewhat imperfect skeleton. Further work will be done to establish general accuracy of our reconstructed map.

3 Applications

We applied our method to a portion of a binary 3D image of pore space in a Vertisol block (Moreau et al., 1999). This 3D image was obtained from an assemblage of sequential 2D images of a fluorescent–dye resin–impregnated block. The initial grey–level 2D images were binarized and then assembled. For the sake of better visualization, only a thin portion of the total pore space of the initial block is shown in Fig. 4a. Each voxel in the initial image represents a cube of 100 micron edge length. The 3D skeleton $\mathcal{S}$ extracted from the initial image is shown in Fig. 4b. The reconstructed image $\mathcal{M}$ using the routines given above is shown in Fig. 4c. It indicates the spatial relations to pore size. Figure 4c shows only three groups of pore sizes for visual clarity. This representation forms a sort of 3D map of the pores as a function of their size.

3.1 Pore size distribution

Pore volume by size distribution can be represented in making a histogram of the size values in $\mathcal{M}$ for individual voxels. Since we work on discrete images, each point P is a voxel representing an elementary pore volume of value 1 in voxels units (or $10^{-3}mm^3$ according to the resolution of the image).

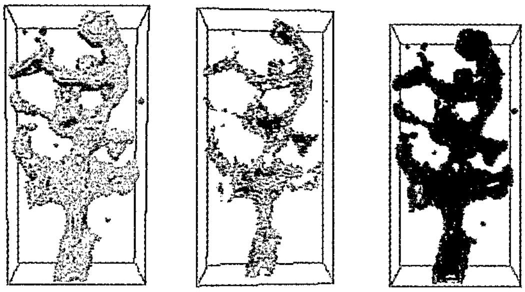

a b c

Fig. 4. Vizualizations of a portion of 3D pore image of a Vertisol (Moreau et al., 1999). a) Original image $\mathcal{P}$ (100*200*20 voxels representing 400mm^3). b) Extracted skeleton $\mathcal{S}$. c) Reconstructed image $\mathcal{M}$.

Each voxel P has been assigned a local pore size $r(P)$ in $\mathcal{M}$. We define any finite number of size classes, and the pore size distribution is described by the histogram of cumulated elementary volumes within each size class (Fig. 5a).

3.2 Simulation of mercury intrusion

The reconstructed pore image or map $\mathcal{M}$ is in fact a cubic network of voxels, where each voxel is associated with a local pore size. Classical methods to simulate a non wetting fluid percolation invasion process (Perrier et al., 1995) in pore networks are adapted to our data to reproduce mercury intrusion in the soil sample : the simulation here processes from voxel to neighboring voxels. Let us consider that mercury enters in a specific area of the soil core, for example from the bottom area shown in grey in Fig. 6a. Then adjacent voxels are filled with mercury if their local pore size is large enough for a given mercury pressure according to Eq. (1). Increasing pressure will allow the fluid to enter subsequently voxels with smaller and smaller local pore sizes, but only if these voxels are connected to the initial area of mercury entry through a continuous path of mercury. Extension of the grey zone in (Fig 6b,c,d) indicates that increased pressure has

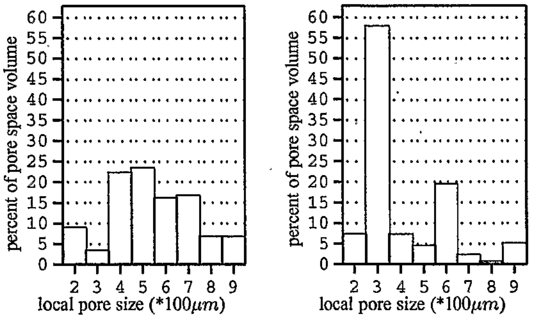

a b

Fig. 5. a) Histogram of the percent pore space volume versus local pore sizes from the reconstructed image of Fig. 4c. b) Same histogram estimated from the mercury injection simulation shown in Fig. 6.

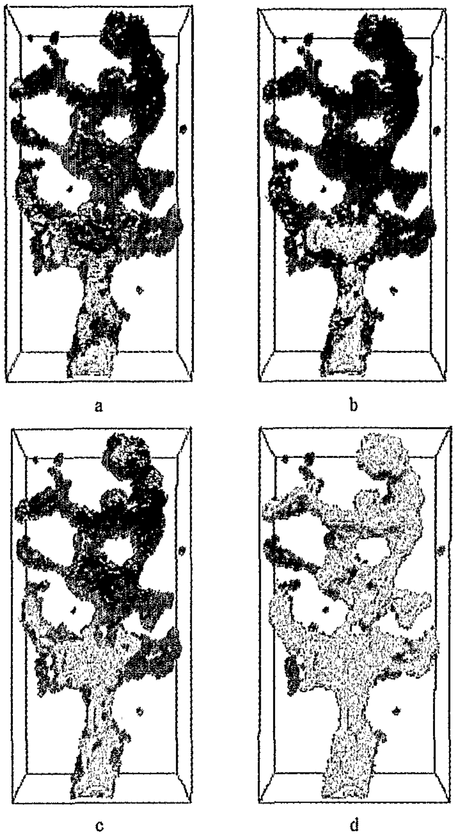

Fig. 6. Representation of mercury intrusion simulation. a, b, c, d) show the initial area of injection and successive invasions using greater and greater "pressures" to invade space limited by increasingly smaller local pore sizes.

allowed mercury to invade smaller and smaller pores. This type of experiment is used to count the volume of pores invaded by mercury at each pressure step and to associate this volume to a given class of pore size. However, connecting pores of small size can lead to filling of larger pores initially unconnected with the point of entry of mercury. Hence, as it is well-known in soil science, the more small pores constrictions prevent full fluid invasion in the whole sample, the more the apparent volume is underestimated in the largest pore size classes and overestimated in the smallest pore sizes. The so-called "equivalent" pore size distribution is shown in Fig. 5b. and can be compared with the "real" pore size distribution (Fig 5a).

4 Conclusion

Use of the Voronoi diagram to determine the pore space skeleton is an important inovative step to calculate pore size distribution both in 2D and 3D media. Local pore sizes are calculated as Euclidean distances instead of linear voxel size as done until now using morphological image analysis.

The determination of a spatialized pore size distribution attributing a local pore size to each voxel of the pore space permits one to depict the connectivity of the pore space through a specific map.

The latter information can be used to perform fluid invasion numerical experiments which can be used to simulate mercury intrusion as done with classical laboratory devices, or to estimate in the same way basic hydraulic properties such as water retention curves

The method is limited by the size of the sample, the resolution of the image and the computing capacity necessary in exploring large images.

It is hoped that after a given number of investigations of pore space in 3D, one can better model pore networks in order to simulate the hydraulic behavior of soils.

References

de Marsily, G., *Quantitative hydrogeology: Groundwater hydrology for engineers*, Academic Press, Orlando, FL, 1986.

Dullien, F. A. L., *Fluid transport and pore structure*, Academic Press, 2nd edn., 1992.

Fies, J. C., Analysis of soil textural porosity relative to skeleton particle size, using mercury porosimetry, *Soil Sci. Soc. Am. J.*, *56*, 1062–1067, 1992.

Guan, W. G. and Ma, S. D., A list-processing approach to compute voronoi diagrams and the euclidean distance transform, *IEEE Trans. on Pattern Analysis and Machine Intelligence*, *20*(7), 757, 1998.

Hallaire, V. and Curmi, P., Image analysis of pore space morphology in soil sections, in relation to water movement., in *Soil Micromorphology : Studies in Management and Genesis Proceedings of 9th International Working Meeting on Soil Micromorphology. Developments in Soil Science.*, edited by A. Ringrose-Voase and G. Humphreys, vol. 22, pp. 559–567, Elsevier, 1994.

Lenormand, R., Touboul, E., and Zarcone, C., Numerical models and experiments on immiscible displacements in porous media, *J. Fluid Mech.*, *189*, 165–187, 1988.

Moreau, E., Velde, B., and Terribile, F., Comparison of 2d and 3d images of fractures in a vertisol, *Geoderma*, in press, 1999.

Perrier, E., Mullon, C., Rieu, M., and Marsily, G. D., Computer construction of fractal soil structiures. simulation of their hydraulic and shrinkage properties, *Water Resources Research*, *31*(12), 2927–2944, 1995.

Perrier, E., Rieu, M., Sposito, G., and Marsily, G. D., Models of the water retention curve for soils with fractal pore-size distribution, *Water Resources Research*, *32*(10), 3025–3031, 1996.

Perrier, E., Bird, N., and Rieu, M., Generalizing the fractal model of soilk structure: the PSF approach, in fractal model in soil science, *special issue of Geoderma*, (1424), in press, 1998.

Pieritz, R. A. and Philippi, P. C., The generalized median line graphics technique in porous media geometry characterization, in *international conference on Quality Control by Artificial Vision*, 1995.

Schmitt, M. and Mattioli, J., *Morphologie Mathematique*, MASSON, collection logique mathematique informatique edn., 1994.

Velde, B., Moreau, E., and Terribile, F., Pore networks in an italian vertisol: quantitative characterisation by two dimensional image analysis, *Geoderma*, *72*, 271–285, 1996.

Washburn, E. W., The dynamics of capillary flow, *Phys. Rev.*, p. 273, 1921.

Xia, Y., Skeletonization via the realization of the fire front's propagation and extinctioin in digital binary shapes, *IEEE Trans. on Pattern Analysis and Machine Intelligence*, *11*(10), 1989.

Yu, Z. Y., Delerue, J. F., and Ma, S. D., 3d euclidean distance transformation, in *Proceedings of the international symposium on Image, Speech, Signal Processing and Robotics*, pp. 67–72, Hong Kong, 1998.

Zida, M., Grimaldi, M., Hallaire, V., Berrier, J., and Curmi, P., Combining image analysis and mercury porosimetry to characterize the pore space of a ferralsols, in *Catena*, 10th International Working Meeting of Soil Micromorphology, Moscow, Russia, 1996.